International Journal of Solids and Structures 45 (2008) 5627–5641

Contents lists available at ScienceDirect

International Journal of Solids and Structures

journal homepage: www.elsevier.com/locate/ijsolstr

Aluminum foam-polymer hybrid structures (APM aluminum foam) in compression testing

Karsten Stöbener [a,*], Dirk Lehmhus [a], Massimiliano Avalle [b], Lorenzo Peroni [b], Matthias Busse [a]

[a] Fraunhofer IFAM, Manufacturing and Advanced Materials, Wiener Straße 12, 28359 Bremen, Germany
[b] Politecnico di Torino, Dipartimento di Meccanica (Mechanics Department), Corso Duca degli Abruzzi, 24, 10129 Torino, Italy

ARTICLE INFO

Article history:
Received 30 October 2007
Received in revised form 27 May 2008
Available online 21 June 2008

Keywords:
Aluminum foam
Mechanical properties
Uniaxial compression
Hydrostatic compression
Deformation behavior
Metal foam-polymer hybrid material

ABSTRACT

The Advanced Pore Morphology (APM) process, a new method for production of aluminum foam-polymer hybrid materials, is described. Small volume aluminum foam spheres are produced first and then adhesively joined in a separate process step to realize an APM foam part. Detailed information on mechanical properties of this new hybrid material is given. Results of uniaxial and hydrostatic compression tests are summarized and evaluated to show how typical parameters characterizing material and process such as spatial arrangement, size and density of the foam elements influence the global properties. Two levels of the hierarchical architecture of the material are evaluated—namely the individual foam spheres and the hybrid structure. Variation of adhesives and adhesive coating thickness used in bonding the spheres in conjunction with study of unbonded specimens provides additional insight in the influence of this bond. First estimates on density dependence of mechanical properties are derived from the experimental data. Distinctive differences between APM and conventional aluminum foams are qualitatively explained. Throughout the study, AlSi7 aluminum foam produced from chemically identical precursor material according to the powder metallurgical FOAMINAL® process is included as reference material.

1. Introduction

Due to their unique property combination of low density, competitive weight specific mechanical properties and high energy absorption capability, aluminum foams can, e.g., be applied in automotive structures to improve their crashworthiness (Rausch and Stöbener, 2006). Among the drawbacks of today's preferred production method, the powder metallurgical Fraunhofer process (FOAMINAL®), which is based on a precursor material incorporating a foaming agent (Baumeister, 1990), are relatively high production costs as well as a certain scatter in material properties. The latter is induced by stochastic influences on the production process which are reflected in the final pore structure, affecting characteristics such as pore size distribution, cell wall shape or degree of cell wall cracking, which in turn impinge on mechanical response (Andrews et al., 1999; Markaki and Clyne, 2001; Issen et al., 2005). The precursor material is expanded in moulds which shape the developing, liquid foam by limiting its growth. During cooling the foam retains its shape until solid and may thus be used without significant post-processing (net shape manufacturing technology). In this process chain the use of foaming moulds increases production costs and limits flexibility, since design evolutions requiring changes in foam part geometry call for a new foaming mould, or an adaptation of the existing one.

* Corresponding author.
E-mail address: stoebener@ifam.fraunhofer.de (K. Stöbener).

0020-7683/$ - see front matter © 2008 Elsevier Ltd. All rights reserved.
doi:10.1016/j.ijsolstr.2008.06.007

With the Advanced Pore Morphology (APM) approach, a new process route has been developed which allows for production of aluminum foam-polymer hybrids without a need for foaming moulds (Stöbener et al., 2005). These hybrids consist of numerous small volume aluminum foam elements with spherical geometry (volume <1 cm^3). Such foam elements can be expanded on a flat surface. Surface tension then draws the liquid foam into a spherical shape. Due to this simple geometry the foam expansion process is well controllable. As a result, high reproducibility of foam density and homogeneity of pore structure is achieved. Coated with a thermoplastic polymer/adhesive, which is non-tacky at room temperature, foam elements can directly be poured into a hollow structure (e.g., automotive A-pillar, sill, etc.). Once the adhesive coating is activated (molten/cured) by low temperature heating (usually below 200 °C), the polymer turns liquid and neighboring elements merge at contact points. In a similar way, adherence of the liquid polymer to the inner surface of the surrounding structure is achieved. After cooling down to room temperature, the solidified polymer forms joints bonding the foam elements to each other and to the inner surface of the shell structure (Fig. 1, middle and right). As a consequence of this simplified process, production may be automated, and flexibility in manufacturing of aluminum foam parts is greatly increased. Both aspects contribute to a significant cost reduction potential in aluminum foam application.

2. Objectives

For application in energy absorption the deformation behavior of the newly developed aluminum foam-polymer hybrids needs to be understood. To provide fundamental knowledge of this kind is the primary objective of the present study.

To this end, experimental results have been gathered on two different levels of geometrical scale, i.e. the levels of the individual foam spheres and of APM hybrid material samples. Uniaxial and hydrostatic testing of selected aluminum foam-polymer hybrid samples shall provide a first insight into the role of the following parameters:

- foam element volume/diameter
- foam element density
- type and thickness of polymer/adhesive coating

A comparison of test results with the deformation pattern of conventionally produced aluminum foams is meant to show if and how the elemental build-up of APM foams governs the respective response of this material.

3. Samples and experiments

3.1. Samples

3.1.1. Aluminum foam elements

The matrix alloy of all investigated samples was AlSi7. Starting from powders, compaction was done according to the CONFORM® process, a specific powder rolling method, to achieve a gas tight and expandable precursor material wire. Foamability was ensured by addition of a foaming agent (0.5 wt% TiH_2) to the initial powder mixture. The precursor material was cut into small volume granules, which were finally expanded into spherical foam elements by heating above their melting point (approximately 700 °C for 3–5 min.) in a continuous belt furnace. The element geometry is not perfectly spherical since gravity forces deform the liquid aluminum foam (situated on the flat furnace belt surface) resulting in an elliptic cross section (Fig. 2). Semi-major axis (parallel to belt surface) is between 14.2% and 20.4% larger than semi-minor axis (perpendicular to belt surface). Average diameter of the investigated foam elements was between approx. 5 and 15 mm.

Fig. 1. Aluminum foam elements of approximately 10 mm diameter (left), foam elements and filled structure (middle) and cross section of automotive transverse control arm with aluminum foam-polymer hybrid core (right).

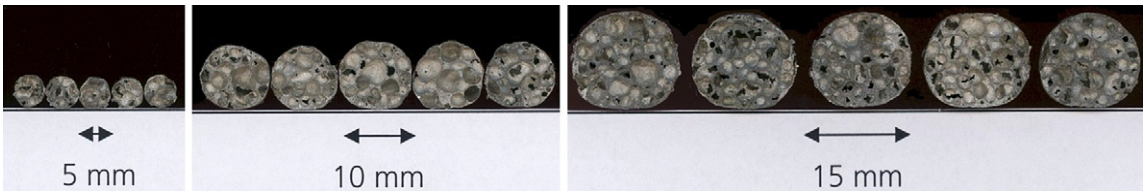

Fig. 2. Cross sections of aluminum foam elements of different sizes but similar overall density.

Fig. 2 further illustrates that the pore size and morphology does not depend significantly on the element volume. Small volume elements therefore contain fewer pores than larger volume elements.

3.1.2. Adhesives and generation of aluminum foam-polymer hybrids

To join the foam elements to each other and thus to achieve the desired aluminum foam-polymer hybrid material two types of adhesive were employed:

Polyamide 12 (short: PA) is a thermoplastic polymer used, e.g., as anti-corrosion coating on metal components. It is a ductile material with 49 MPa tensile strength and 311% elongation at break. Mechanical properties under compressive load were not available to the authors. PA 12 melts at 176 °C and wets aluminum surfaces well (Degussa, 2004).

Araldite AT 1-1 (short: EP) is a single component thermoplastic reaction adhesive (epoxy) used for structural bonding. It exhibits 34 MPa tensile transverse resistance and 68 MPa elastic compression limit. Melting of Araldite AT 1-1 is initiated at 70 °C, while curing starts at 120 °C, following which the material remains thermally stable up to 180 °C (Vantico, 2001).

For coating, foam elements were heated well above the melting point of the employed adhesive and poured into a fluidized bed of adhesive powder (fluidized by compressed air supply). Once the polymer particles make contact with the hot foam element surface, they melt and build up a surface film. The coating thickness can be adjusted via the foam element temperature prior to entering the powder bed. Coating with the PA adhesive was done in three different thicknesses, but maintaining a constant ratio between coating thickness b and foam element diameter D ($b/D = 5 \times 10^{-3}$; 15×10^{-3} and 29×10^{-3}). With the EP adhesive one coating thickness ($b/D = 10 \times 10^{-3}$) has been realized.

For production of the aluminum foam-polymer hybrids, coated foam elements were poured into cylindrical moulds. The random element arrangement was densified by means of vibration. By subsequent heating to approximately 180 °C the coating was molten and cured (the latter only in the case of EP). The liquid polymer coatings merge at contact points between neighboring foam elements, finally constituting solid polymer joints between foam elements. Adhesion to the mould surface was inhibited using PTFE foil. Activation of the adhesive results in a further densification of the random foam element arrangement up to a level of 10%, depending on the coating thickness. This effect can be explained by assuming that under the influence of gravity the liquid polymer coating is displaced at contact points between neighboring foam spheres. The effective foam element diameter thus decreases to the level associated with the uncoated foam elements, leading to the observed volume reduction. In the course of this process, new displacement paths may be opened for a rearrangement of the spheres, a development which will once again lead to higher packing density.

According to this method samples for mechanical testing were produced from adhesive coated aluminum foam elements with diameters of approximately 5, 7, 10 and 15 mm. A circular aluminum extrusion profile has been employed as mould to shape the aluminum foam-polymer hybrid samples in cylindrical geometry (diameter = 50 mm) during the adhesive bonding processing step. Contact and adhesive bonding of foam elements to the inner surface of the profile has been inhibited by a thin PTFE foil. Samples were finally cut to lengths of 75 mm for uniaxial and 50 mm for hydrostatic testing.

3.1.3. Reference samples

As reference material, conventional Fraunhofer type AlSi7 foam (Fig. 3) samples were produced from precursor material identical in chemical composition to that used in the making of small volume aluminum foam elements. Compaction was based on cold isostatic pressing and subsequent hot extrusion of the powder mixture (FOAMINAL® process). The samples tested were cubic with dimensions of $41 \times 41 \times 41$ mm^3 for uniaxial compression and cylindrical with 41 mm diameter at 41 mm height for hydrostatic testing. They were cut from larger samples in order to remove the closed skin usually developed in this kind of foam during expansion and in contact with the mould. A detailed review of an extended test program performed on conventional aluminum foam samples of this kind has been provided by Avalle (Avalle et al., 2004).

3.2. Test procedures

3.2.1. Uniaxial compression testing

Single foam elements as well as adhesively bonded aluminum foam-polymer hybrid samples were tested in a universal testing machine (Zwick A 1472) between two flat and parallel plates. In a second test series loose foam elements (bulk) and adhesively bonded aluminum foam-polymer hybrid samples were subjected to confined compression in a cylindrical die. Testing samples in a closed die almost completely inhibits transverse straining more comparable to foam application as core in shell structures. The aluminum foam-polymer hybrid samples diameter was approximately 0.1–0.2 mm smaller than the

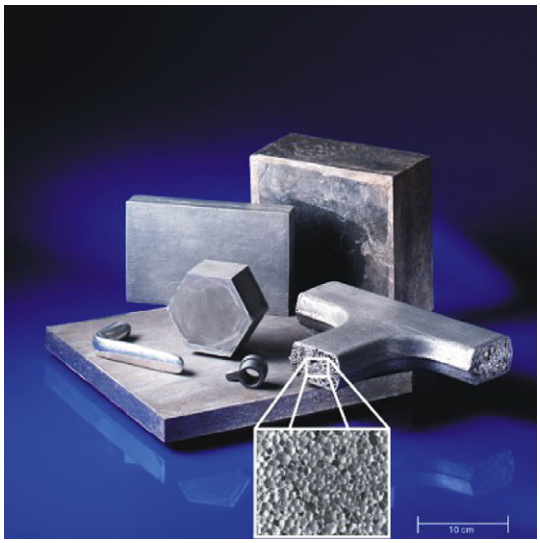

Fig. 3. Reference material: FOAMINAL® aluminum foam (closed cell porosity, closed surface skin).

inner diameter of the test die. This minimum space for transverse straining (max. 0.4%) must be taken into account when interpreting test results from confined compression. Initial modulus and yielding are mainly affected by this transverse straining. Consequently, the initial modulus has not been analyzed. For analysis of the transition from quasi-elastic to plastic deformation (yielding) sample transverse straining needs to be considered. In all confined compression tests, the inner die and stamp surfaces were coated with high pressure resistant lubricant. Remaining forces from friction between sample and die, as well as between stamp and die, can in principle affect the experimental measurements and cannot be extracted, since no exact values of either friction coefficients or Poisson's ratio of the aluminum foam-polymer hybrid sample material are available. Effects of this kind will be discussed qualitatively in the results section (chapter 4).

3.2.2. Hydrostatic compression testing

Hydrostatic compression tests were performed only on selected sample types with foam element diameters of 7 and (predominantly) 10 mm.

The tests were executed by means of a custom made test chamber consisting of a steel tube (140 mm external diameter, 90 mm internal diameter) closed by a couple of flanges fastened by a series of bolts (Fig. 4). The chamber is filled with a nearly incompressible fluid, namely water with added ethylene glycol. Pressure is generated by the relative movement of two rods connected to a general purpose hydraulic testing machine (DARTEC HA100, with 100 kN maximum load, 0.1 m/s maximum speed, 100 mm travel). The rods, one fixed, the other sliding into the chamber, pass through sealed holes in the test chamber flanges. The pressure, which is also the hydrostatic stress applied to the sample, is indirectly measured by means of the machine load cell. Some direct measurements of the pressure inside the chamber were also performed: since low friction seals are adopted, the differences observed in comparison to the indirect measurements were negligible. Therefore, in the present tests only indirect measurements were used. The volumetric strain is related to the stroke of the rod into the chamber. To compensate for the remaining, though very low, compressibility of the fluid, correction curves have been measured and accounted for in all subsequent measurements.

To exert a hydrostatic stress on the sample the loading fluid must be completely separated from it. Otherwise the individual spheres, or the base material itself in the case of open cells, rather than the foam will be loaded in hydrostatic compression. The separation was practically obtained using a strong PVC sheath internally and an external latex pouch. The PVC jacket was necessary to avoid tearing of the latex pouch.

Fig. 5 shows a foam sample before insertion into the chamber, and two (one PA and one EP bonded) samples after the test. A simple visual examination reveals the inhomogeneous deformation of the sample caused by the specimen geometry and, to a lesser extent in this case, material anisotropy.

4. Results

4.1. Unconfined uniaxial compression

4.1.1. Aluminum foam elements—experimental results

Individual aluminum foam elements differ from samples usually tested in being of spherical or ellipsoidal geometry. The contact area between element and stamps depends on sample deformation. Fig. 6 depicts a foam element (D = 10 mm) at

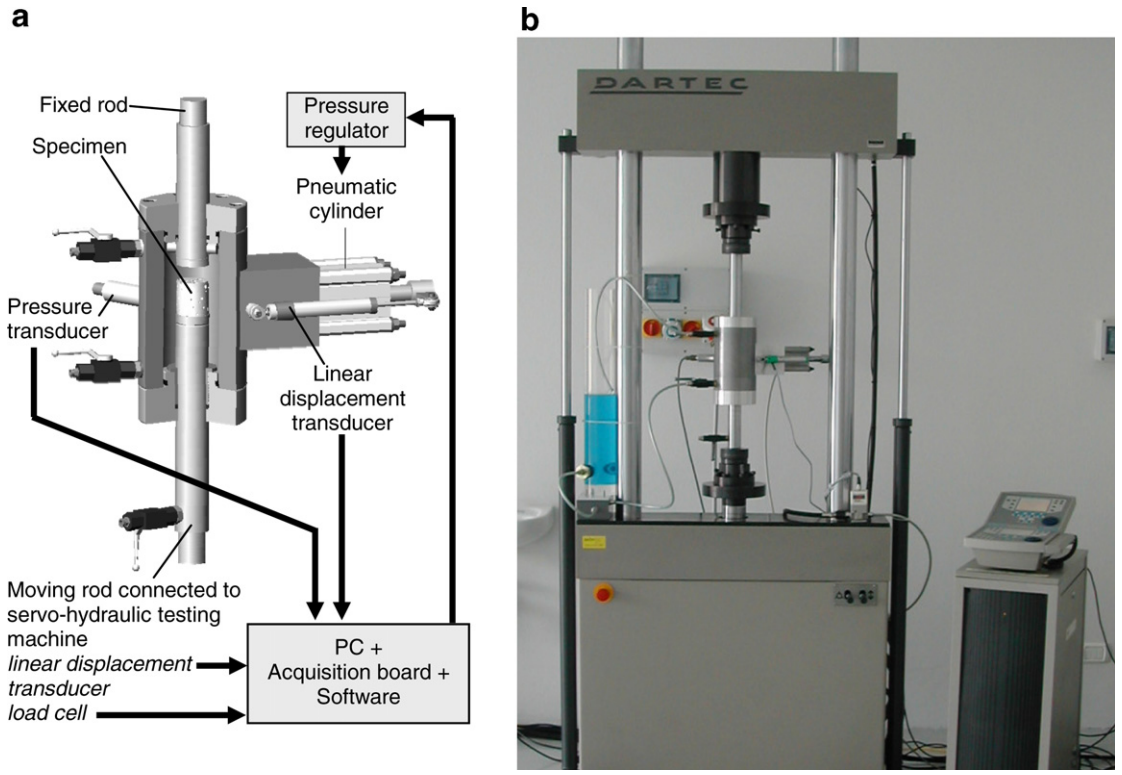

Fig. 4. Test chamber for hydrostatic tests: (a) schematic representation of the system (left); (b) the test chamber mounted on the DARTEC HA100 testing machine (right).

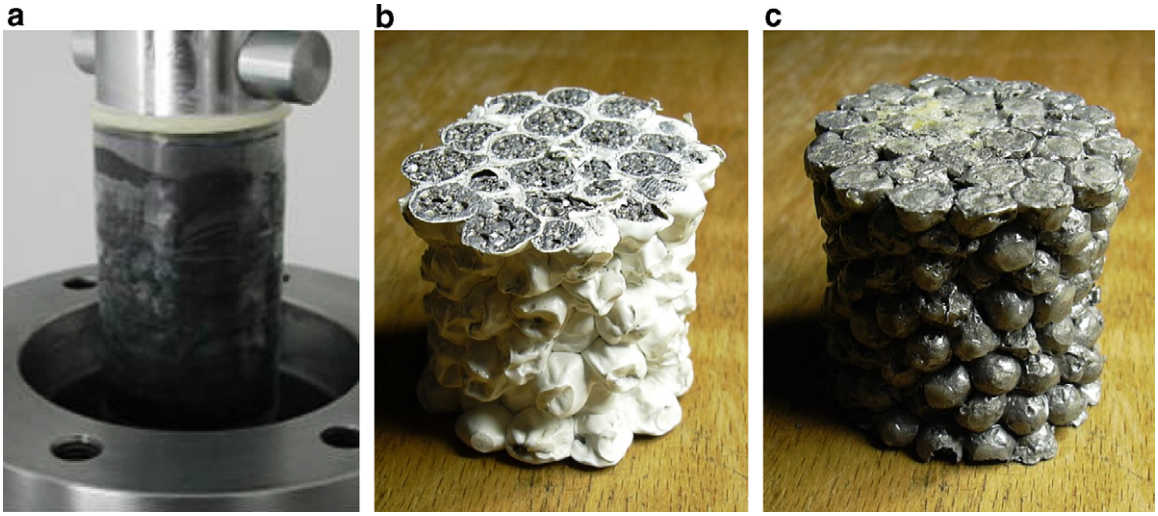

Fig. 5. (a) An aluminum foam-polymer hybrid sample just before insertion in the hydrostatic loading chamber (left); (b and c) APM foam sample after the hydrostatic test (middle: $D = 10$ mm, Polyamide 12, $b/D = 29 \times 10^{-3}$, 0.41 g/cm^3; right: $D = 10$ mm, Araldite AT 1-1, $b/D = 10 \times 10^{-3}$, 0.41 g/cm^3).

various global compression states (in the following, global compression or global compressive strain are defined as stamp deflection related to semi-minor axis of the elliptical cross section parallel to loading direction). The stamps flatten the former, near spherical shape. At 60% global compression cracking of the formerly closed surface skin is visible. Occurrence of similar effects at lower strain levels is possible, but cannot be directly observed owing to the deformed geometry.

Associated force-compressive strain curves are shown in Fig. 7, where different aluminum foam densities and element diameters are contrasted. Naturally, higher density increases the force level at constant element volume. Larger foam element volume also resulted in increased deformation resistance and force levels.

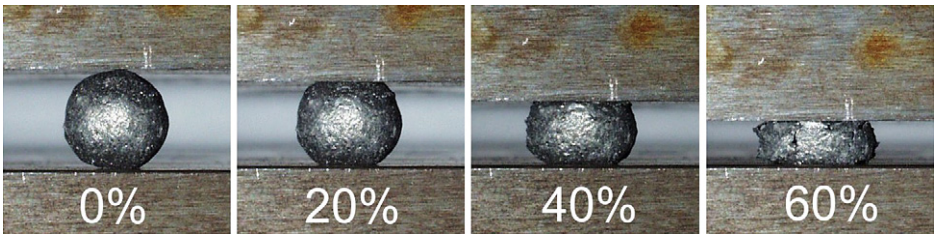

Fig. 6. Compression states of a single aluminum foam element (D = 10 mm) in uniaxial compression.

Obviously, the cross section in the direction of loading is non-uniform. Deformation is likely to start at the contact points between loading plates and specimen, i.e., foam sphere. The element is then progressively compressed, with plastic straining occurring primarily in the momentarily smallest cross sectional area. Fig. 6 perfectly reflects this pattern: The initial ellipsoid is effectively flattened from both load introduction points towards the centre plane. Several other aspects are superimposed to this general behavior. Acting in part against the described course of events is strain hardening, since it serves to strengthen those areas within the foam which suffer the highest levels of deformation. Besides, like conventional aluminum foams, the foam spheres are characterized by a closed outer skin, which constitutes a density gradient from core to surface. An additional structural resistance from this skin is expected but cannot be quantified due to irregular shape and interaction with the cellular structure in the element volume.

An average global compressive stress in the plateau region (between approx. 20% and 40% global compressive strain) is estimated by relating compressive forces to the contact area between deformed foam element and stamp (Fig. 8). This contact area is estimated from the base area of the deformed ellipsoid segment. Comparison with experimentally determined contact areas has proved sufficient accuracy of this area approximation. Average compressive stress values determine a power law dependency on the relative foam density σ_{rel} (eq. 1; C = material constant, $n \approx 1.5$) as developed by Ashby et al. (2000) for conventional closed cell aluminum foams. A significant influence of the foam element volume/diameter on the stress level is not substantiated. Average global compressive stresses are marginally lower than those of larger volume but equal density aluminum foam (FOAMINAL®) samples. This minor discrepancy is not attributed to element volume or geometry. It is considered more likely, that the accuracy of the chosen stress approximation is limited.

$$\sigma = C \times \rho_{rel}^{n} \tag{1}$$

4.1.2. Aluminum foam-polymer hybrid materials—experimental results

Testing of APM foams under uniaxial loads between two parallel load plates gives a first insight into the basic deformation mechanisms of this hybrid material and confirms a major role for all components of the hybrid. Adhesive joints between foam elements turned out to be of primary importance for the overall deformation pattern, whereas foam element volume and density had no influence in this respect. PA bonded samples with highest polymer coating thickness ($b/D = 29 \times 10^{-3}$) deformed as a continuum (Fig. 9).

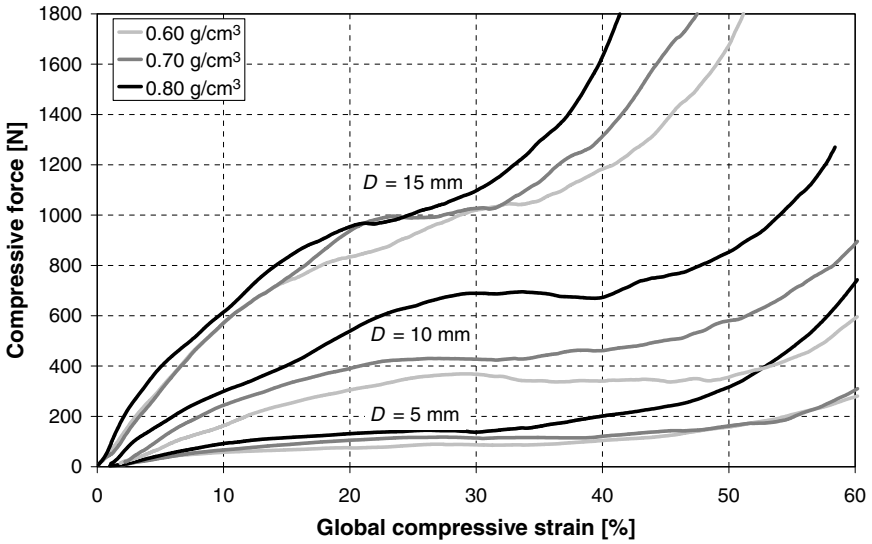

Fig. 7. Compressive force vs. global compressive strain of different aluminum foam elements in uniaxial compression.

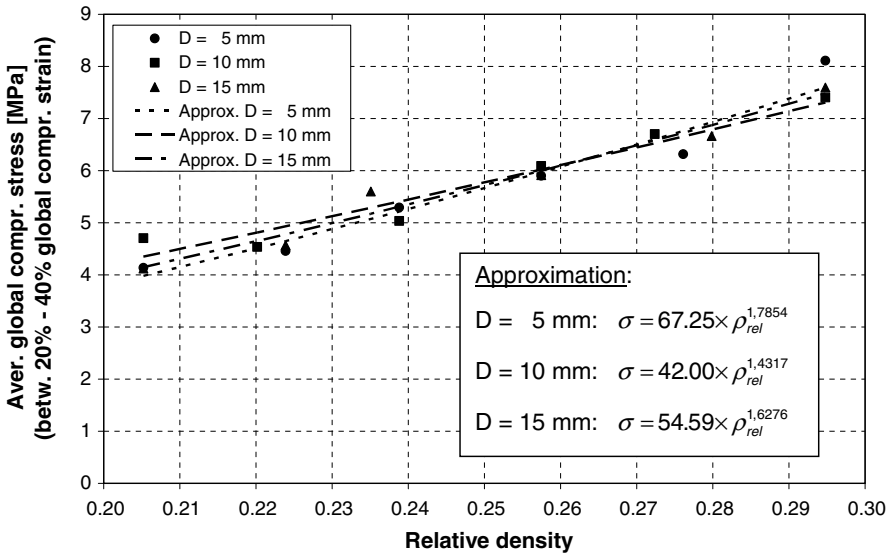

Fig. 8. Average global compressive stress vs. relative density determined from uniaxial testing of foam elements with different volumes/diameters and power law equations as linear approximation.

A reduction of the PA coating thickness ($b/D = 5 \times 10^3$ and $b/D = 15 \times 10^{-3}$) weakened the joints between the foam elements, resulting in disintegration of the hybrid structure at low global strain levels (Fig. 10, left). In this failure mode, the separation planes lie within the polymer and thus between foam elements. Bonding foam elements via the alternative epoxy resin (Araldite AT 1-1) leads to a third deformation pattern. The sample volume is first compressed as a continuum. Starting at approximately 35–40% global strain, macroscopic cracking occurs. In this case, the polymeric joint is stronger than the aluminum foam: Cracks run through the foam element volume (Fig. 10, right).

Fig. 11 displays compressive stress vs. global compressive strain graphs of two representative samples which did not disintegrate during compression. An influence of the adhesive type and/or coating thickness on the stress level is distinguishable and matches qualitatively the relative tensile strength of the adhesives as specified by the suppliers (see chapter 3.1.2). For EP bonded samples, local cracking of aluminum foam elements started at approximately 35–40%. Thus, global compressive strain caused a loss in deformation resistance resulting in a decreasing nominal stress level.

Compared to the plastic response, elastic properties even of conventional aluminum foams are difficult to establish, since the initial slope of the stress–strain curve in uniaxial compression of aluminum foams is not truly of elastic nature (Ashby et al., 2000). It is known, for example, that closed cell foams show direct plastic deformation in the pore structure at defects, irregularly shaped pores, etc. (Huschka et al., 1997; Simancik et al., 1997; Degischer and Kottar, 1999). Ashby et al. (2000) therefore recommend determining the stiffness (Young's modulus) from the slope of an unloading curve. In following this procedure, aluminum foam-polymer hybrid samples were unloaded at defined compression states (5%, 10%, 20%, 30%, 40% and 50%) during uniaxial compression between two flat plates. Fig. 12 displays average stiffness in terms of an elastic modulus determined between 5% and 30% global compressive strain on samples that did neither disintegrate nor crack. All these values are approximately one order of magnitude higher than the initial slopes of the associated experimental stress–strain curves. Type of coating, coating thickness and sample density are the main influencing factors. Increasing coating thickness or foam element density resulted in a stiffness increase. In contrast, the volume/diameter of the employed foam elements did not show a direct influence. Stiffness also increased with accumulated sample compression (>30%). Results

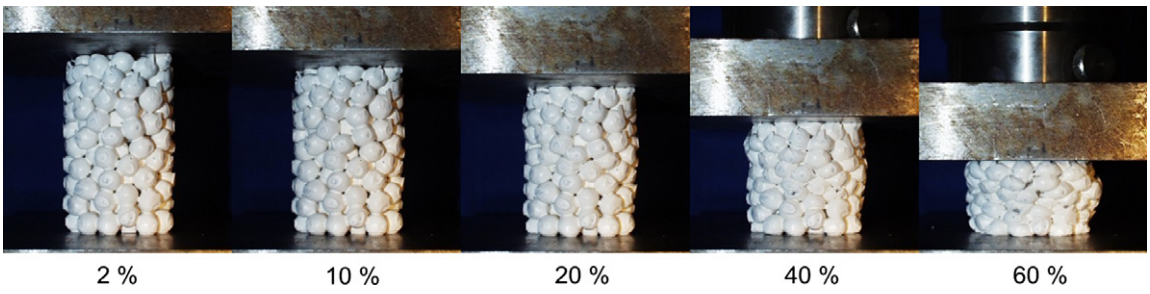

Fig. 9. PA bonded APM foams ($b/D = 29 \times 10^{-3}$) during uniaxial compression (nominal engineering compressive strain chosen as strain measure).

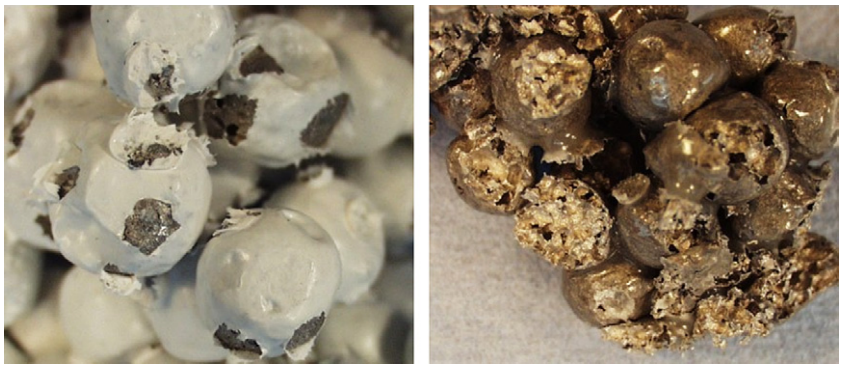

Fig. 10. Failure of adhesive bonding (left; PA; $b/D = 5 \times 10^{-3}$and $b/D = 15 \times 10^{-3}$) and rupture within the aluminum foam element volume (right; EP, $b/D = 10 \times 10^{-3}$).

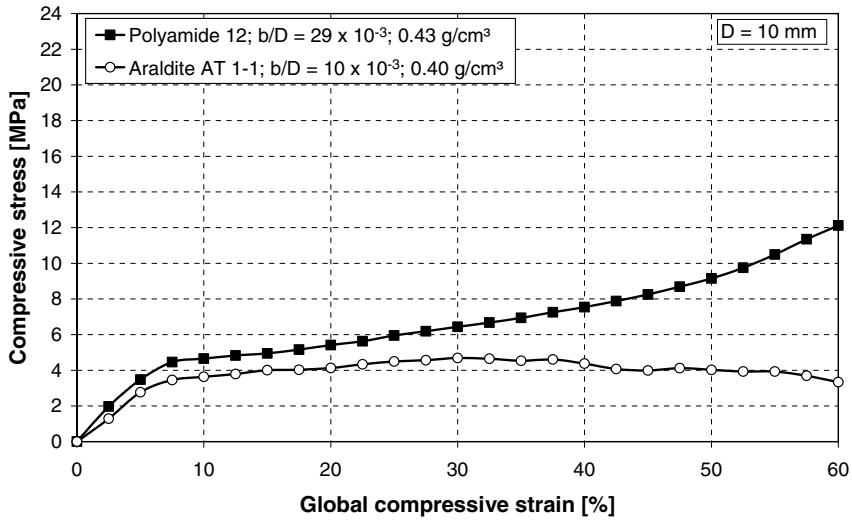

Fig. 11. Compressive stress vs. global compressive strain response of selected samples in uniaxial compression.

gathered at this and higher levels of deformation have not been considered for calculation of average stiffness values since here the characteristic inner sample structure and specifically the fraction of interconnected porosity between foam elements is almost completely densified. Experiments of this kind have been performed on conventional aluminum foams of the same matrix alloy in the past (Avalle et al., 2004). From these, the elastic modulus can be estimated to be 1595 MPa for a density of 0.4 g/cm^3 and 3589 MPa at 0.6 g/cm^3 assuming a scaling of stiffness with the square of density, as has been suggested by Gibson and Ashby (Gibson and Ashby, 1997). Using the same dependency on density squared, the tangent modulus or maximum slope of the stress–strain curve in the elasto-plastic region turns out to lie between 266 and 597 MPa for conventional aluminum foam in the same density range. On average, weight specific stiffness of these foams is thus at least twice as high as that of APM materials when looking at results gained from unloading/reloading cycles. An explanation may once more be based on the elemental build-up of the hybrid material and the consequential progressive deformation of the individual foam spheres. The fact as such is put into perspective, though, by the exceedingly high scatter of data observed in the stiffness evaluation of conventional aluminum foams.

4.2. Confined uniaxial compression

Further investigations of the deformation behavior of aluminum foam-polymer hybrids have been conducted under conditions of confined compression. The samples were uniaxially compressed in a closed cylindrical steel die between two steel stamps. This experimental configuration allowed for additional testing of pure aluminum foam element bulks without adhesive bonding, since the die enclosed the sample volume completely. Samples (not bonded and adhesively bonded foam elements) were prepared from foam elements with diameters 5, 10 and 15 mm. For samples made from larger elements (10 and 15 mm) the cylindrical test cavity (diameter = 50 mm, height = 75 mm) was only coarsely filled and random element

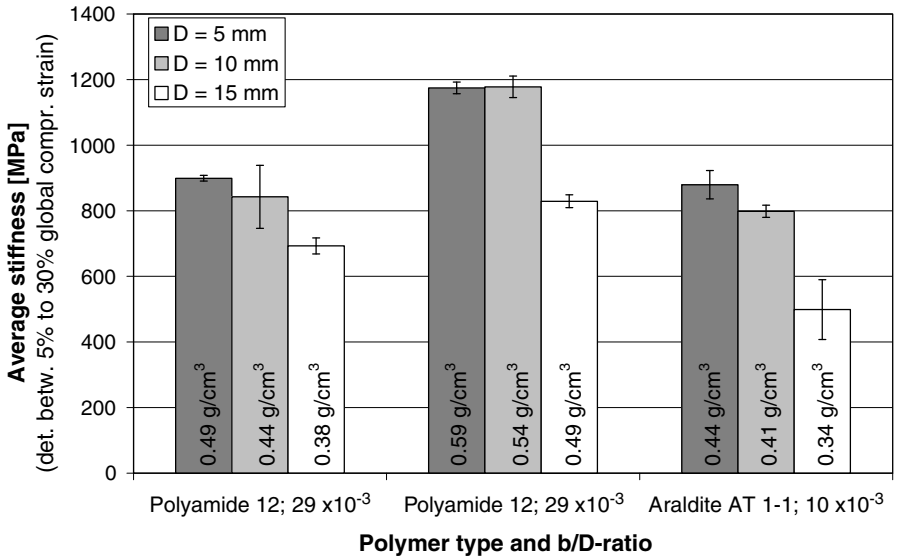

Fig. 12. Average stiffness of aluminum foam-polymer hybrid samples, determined from unloading curves at defined levels of global compressive strain.

arrangement might have been disturbed by fringe effects. However, no significant effect of the foam element diameter/volume on the results of confined uniaxial compression testing has been observed in the present study.

Foam element bulks responded to confined uniaxial compression with an almost linear stress increase, which changes at approximately 40–50% compression to exponentially increasing (Fig. 12). An expected initial stiffness (elastic deformation mode) could not be identified. The bulk of foam elements seem to deform plastically beginning with initial loading.

An inadequate compaction of the foam element bulk prior to testing is one potential reason for the observed stress–strain response. Uniaxial loading would result in densification of the element packing and overlap with elastic deformation of the foam elements. Both processes run parallel leading to the observed linear global stress–strain response.

Assuming an adequate element compaction (since all element bulks have been compacted by means of vibration in the die prior to testing) an alternative explanation for the observed stress–strain response is developed. Spherical foam elements are in point contact to their closest neighbors with very small initial contact area. Global loading of the element bulk generates comparably high stresses in the contact areas. Naturally, the element volume underneath the contact area is first elastically deformed. The inner structure of a foam element (Fig. 2) indicates that stiffness and yield strength of the thin element surface skin and inner cell walls (underneath) should be comparably low. In the measured global stress–strain response of the not bonded foam element bulk the elastic deformation mode might not be identifiable in the stress–strain curvature due to its very small extent. Further, (elastic or plastic) deformation of elements opens degrees of freedom for rearrangement and densification of packing. This process also impacts on the global stress–strain curvature and impedes identification of the elastic deformation mode.

The performed confined compression of loose foam element bulks has high analogy to metal powder compaction in closed cylindrical dies. In both cases random arrangements of spherical particles/elements are subjected to confined uniaxial compression. Fleck (Fleck, 1995) as well as Heylinger and McMeeking (Heylinger and McMeeking, 2001) investigated mechanics of random metal powder particle arrangements in confined uniaxial compression. Neglecting friction (between sample and die) and assuming ideal plastic deformation behavior of the metal powder particles (no elastic deformation) finally delivered a linear global stress increase as a first approximation. This result is in good agreement with confined foam element bulk compression results of this study, the more so since metal foam deformation behavior clearly resembles the ideal plastic approximation as long as the densification region is not reached (see Fig. 18). This, however, is not the case for the present material up to strain levels between 40% and 50%. The assumption that the elastic deformation mode of not bonded foam element bulks is too small to be clearly identified in the global stress–strain curvature is underlined.

Irrespective of the reason for the linear stress–strain response of not bonded foam element bulks to confined uniaxial compression the primary goal of this test configuration was the comparison of mechanical behavior of not bonded and of adhesively bonded samples under similar test conditions. Even in the case elements were compacted inadequately this condition applied to not bonded and adhesively bonded samples in the same way since processing and testing has been identical in all cases. Practically, this means that a comparison among experiments of this type is valid.

Adhesive bonding of foam elements led to a distinct change in the global stress–strain response to confined uniaxial compression (Fig. 13). An initial quasi-elastic deformation mode is followed by plastic deformation with a rather smooth transition between both modes. Adhesively bonded foam elements are fixed in their position and cannot rearrange. Contact to neighboring spheres is associated with a defined area and, e.g., controlled by the coating thickness. The coating itself is con-

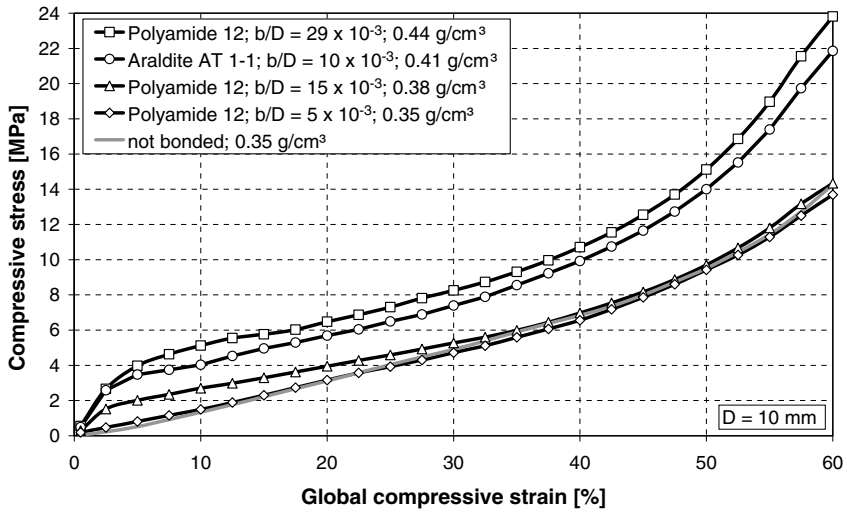

Fig. 13. Compressive stress vs. global compressive strain in confined uniaxial compression of loose foam elements and different types of aluminum foam-polymer hybrids.

tinuous and envelopes the neighboring spheres as well as the joint. Shear stresses perpendicular to the normal of the separation plane can thus be transmitted from sphere to sphere through this plane. Keeping friction out of consideration, this is not possible among loose spheres. Under compressive loads both the polymer joint and the adjacent aluminum foam spheres are first deformed quasi-elastically. Localized plastic deformation in the pore structure of the aluminum foam is possible but not dominant; hence the term "quasi-elastic behavior" is used. The same holds true for the initiation of plastic yield at contact points as described above. With increasing compressive force, the elastic deformation limit of the polymer joint and the aluminum foam is reached. Plastic deformation in both components dominates the stress–strain response from this point onwards and results in a slower stress increase. Fig. 12 further substantiates that the type of adhesive and the coating thickness influence the stress level in compressive testing. With increasing bond strength, i.e., with increasing coating thickness, higher deformation resistance is observed. At the same time, the general shape of the stress–strain curve approaches that of conventional aluminum foams in showing a clear distinction between the quasi-elastic and subsequent failure modes. Beyond this transition, stress–strain curves of loose foam elements and joined aluminum foam-polymer hybrid samples develop qualitatively similar in plastic deformation. Adhesive bonding of foam elements raises the deformation resistance and, thus, the stress level but does not change general plastic deformation mechanisms significantly.

The precise point of transition from quasi-elastic to plastic deformation is difficult to quantify, the process being gradual. Linear approximation of quasi-elastic and plastic regions of the stress–strain curvature delivers a point of intersection described by the elastic compression limit ε_P and stress σ_P (Fig. 14). As boundaries for interpolation, 0.5% to 2.0% (quasi-elastic) and 10% to 30% global compressive strain were selected.

A quantitative evaluation of both characteristics (ε_P; σ_P) as well as weight specific energy absorption reveals a dependency primarily on sample density. Further influence is attributable to type and thickness of the polymer coating. Highest values of σ_P and ε_P are observed for samples having greatest density and coating thickness (Figs. 15,16). For the PA bonded samples with a b/D-ratio of 29×10^{-3}, the experiments allow direct comparison of different sphere sizes. For the strain measure, the issue is unresolved, while stress levels seem to be higher in samples built up from smaller elements. However, due to the scatter of data, which is much higher among the stress compared to strain values, no clear statement can be derived. Density scaling is also more evident among strain values. Altogether, aluminum foam-polymer hybrids show compression properties and density dependence similar to closed cell aluminum foams (Ashby et al., 2000). Opposing σ_P values to similarly derived strength values of conventional aluminum foam based on the same matrix alloy yields similar results as in the case of elastic properties: The conventional foam outperforms the hybrid material in absolute figures. The margin, however, is negligible for low densities, with a compressive strength of 3.9 MPa recorded for a density of 0.4 g/cm^3 and 9.0 MPa at 0.6 g/cm^3 (Avalle et al., 2004). The latter exceeds the APM foam value by a factor of less than 1.4.

In terms of weight specific energy absorption, PA bonded samples with highest foam density and polymer coating thickness yield best performance within this test series. Based on the assumption that influence of the element size may be neglected, Fig. 17 shows dependence of the amount of energy absorbed from the density. For reasons of clarity, linear fit curves have been provided for the various data sets. In this diagram, vertical translations of curves denote the influence of the adhesive, while the inclination is mainly due to the density dependence of aluminum foam strength. Comparison of PA bonded samples shows that a certain coating thickness is needed to heighten energy absorption levels. The steeper gradient found for PA bonded samples with a b/D-ratio of 29×10^{-3} is probably a consequence of the larger density range covered by these specimens, which leads to a more obvious expression of the power law linking foam strength to density. The example of the

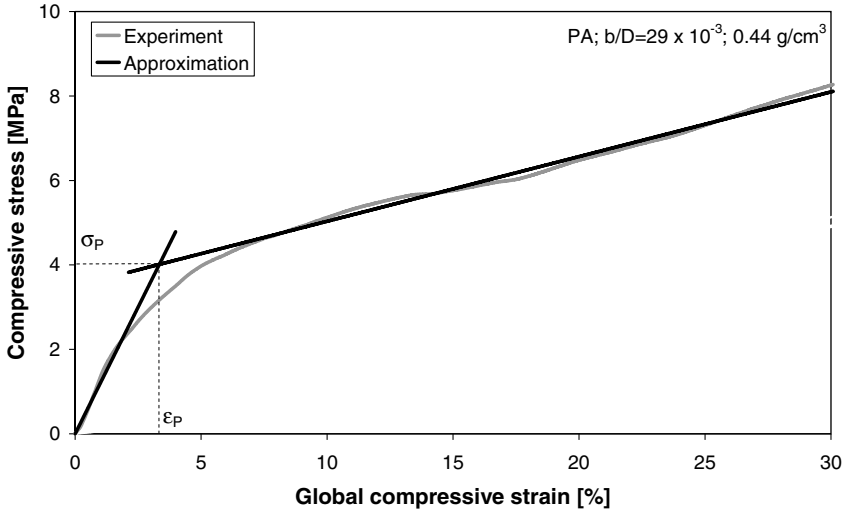

Fig. 14. Definition of the elastic compression limit ε_P and associated stress σ_P.

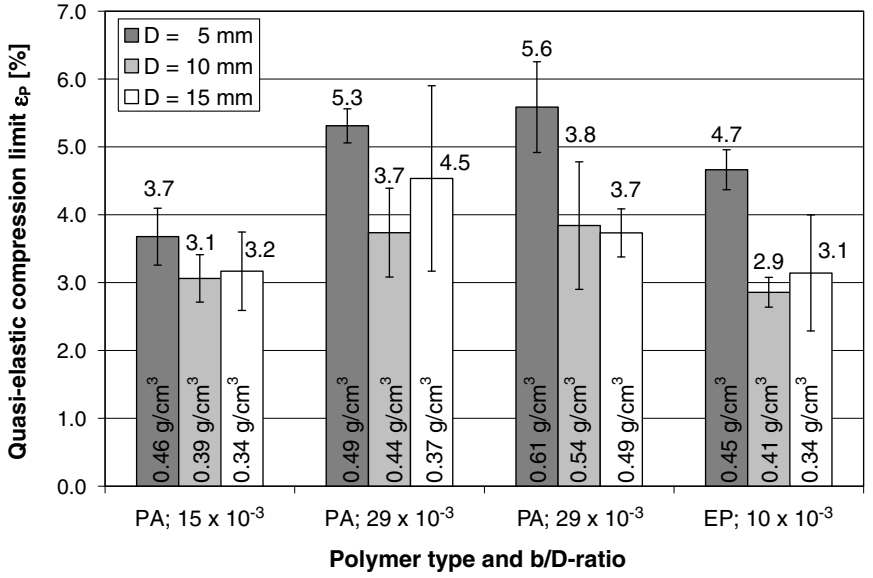

Fig. 15. Compression limit for quasi-elastic compression of adhesively bonded APM foams.

EP bonded samples shows that superior strength of the adhesive can be used to tailor energy absorption, too. This hybrid variant clearly outperforms PA variants with higher coating thickness at the same density.

Fig. 18 compares representative results from both tests series performed on aluminum foam-polymer samples and, as reference, the result from unconfined uniaxial testing of closed cell aluminum foam (FOAMINAL®). Up to approximately 15% global compressive strain level the different testing conditions did not influence the stress–strain response of the hybrid samples significantly. In these very early compression states transverse straining of the sample and friction forces are negligible in terms of stress–strain curvatures and analyzed characteristics. At higher compression levels the inhibited transverse straining and additional friction forces in confined compression of these samples result in a more pronounced stress increase for the confined sample.

Generally, aluminum foam-polymer hybrids show a stress–strain curve similar to closed cell aluminum foams (FOAMINAL®) of comparable density. However, for similar test conditions (un-confined compression) initial stiffness and stress level in plastic deformation are significantly lower. This is related to the additional open porosity in aluminum foam-polymer hybrids, i.e., the space between the spherical foam elements which is virtually eliminated at approximately 20–30% global compressive strain. Up to this point, contact area effects as described earlier will influence the expression of the stress–strain

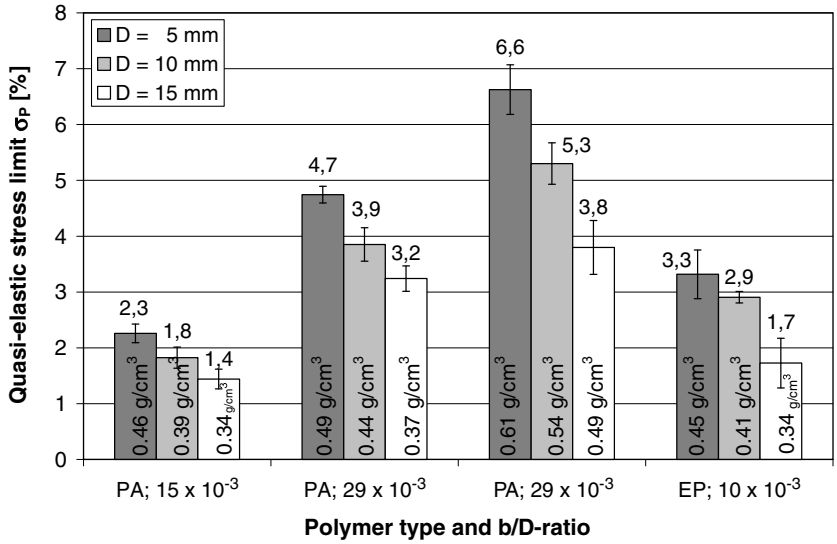

Fig. 16. Compressive stress at compression limit for quasi-elastic compression of adhesively bonded APM foams.

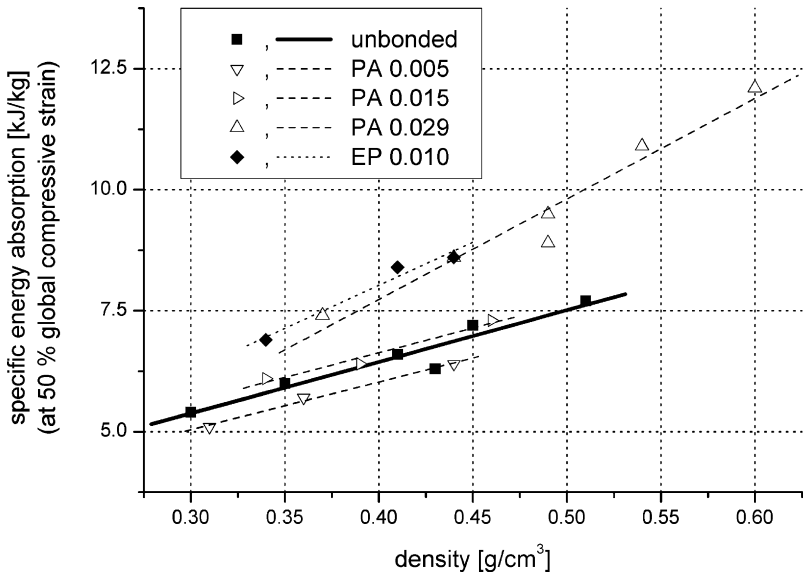

Fig. 17. Weight specific energy absorption (at 50% global compressive strain) of loose foam elements and adhesively bonded aluminum foam-polymer hybrids as a function of density.

curve, adversely affecting the global stress level. Beyond it, Fig. 18 testifies, within the limits of accuracy induced by scatter, to an identical course of deformation for both materials. The slight advantage of the hybrid in confined compression in terms of steepness of later stages of the stress–strain curve may be due to transverse straining and resulting friction between specimen and die wall. Further investigations are required to gain more insight into the importance of this effect and its quantitative contribution to the stress response.

4.3. Hydrostatic compression

Hydrostatic compression test results are shown in Fig. 19. An obvious difference to the uniaxial compression test is the lack of a clearly defined plateau. The same phenomenon was observed in hydrostatic tests on several other cellular materials (Peroni and Avalle, 2007; Ruan et al., 2005; Ashby et al., 2000; Nusholtz et al., 1996).

As Fig. 19 evidently shows, the results are sufficiently repeatable among different samples of each material variant. In Fig. 20, a direct comparison between them is shown. For simplicity, a single, average, curve is shown for each material. Ex-

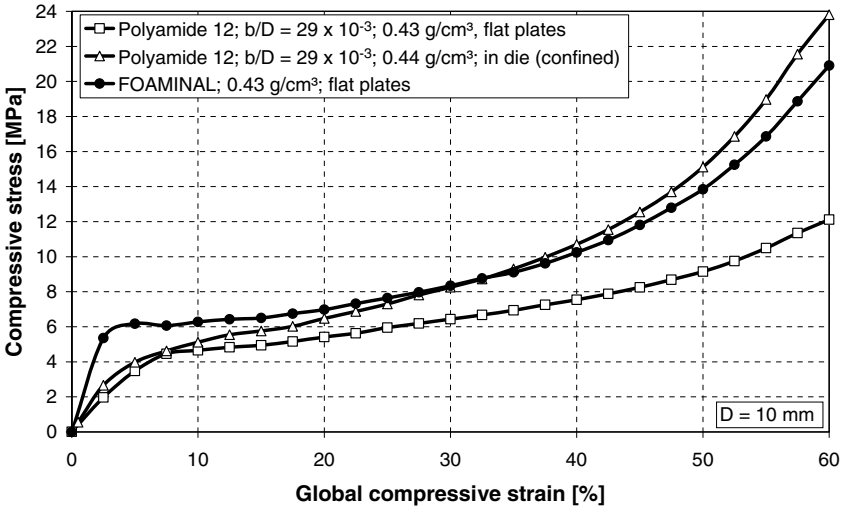

Fig. 18. Comparison of response to uniaxial compression measured on aluminum foam-polymer hybrids and closed cell aluminum foams (FOAMINAL®).

cept for the high-density foam bonded with PA, the first, quasi-elastic, part of the curve is not affected by both density and adhesive type. In the second region, and towards densification, the PA bonded APM foams are significantly stiffer. This effect is in good agreement with observations made on conventional aluminum foams in uniaxial compression. Typically, ductile matrix materials (which would match, in terms of deformability, the PA as opposed to the EP bonded samples in this com-

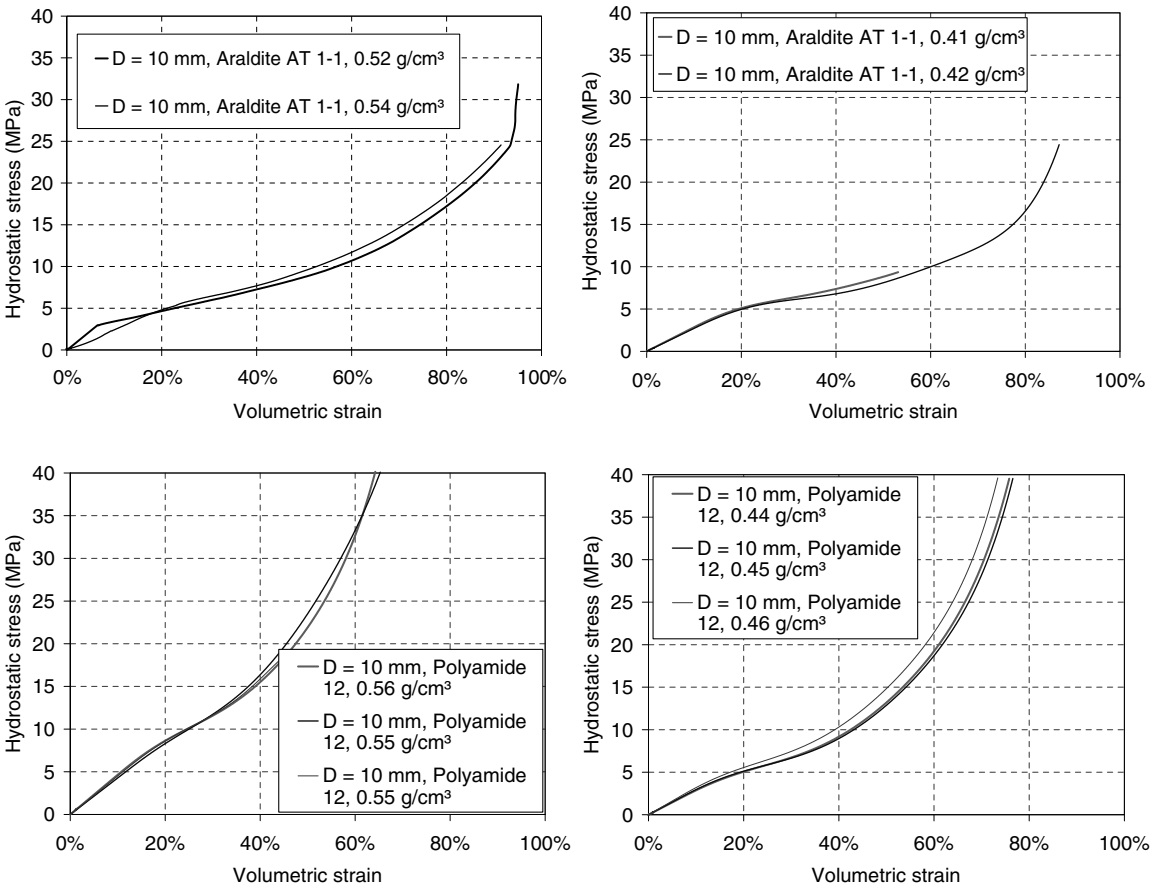

Fig. 19. Hydrostatic compression test results measured on aluminum foam-polymer hybrid samples (EP and PA bonding, each test at two densities).

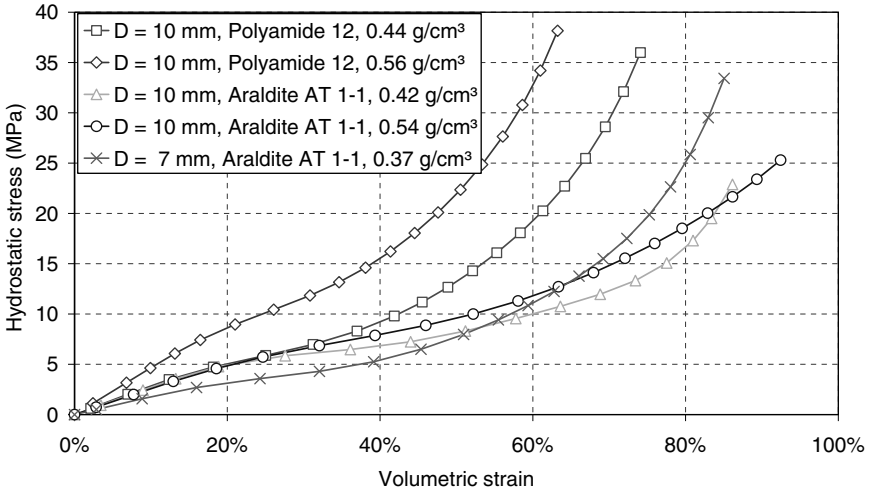

Fig. 20. Comparison of the hydrostatic test results on different APM foams.

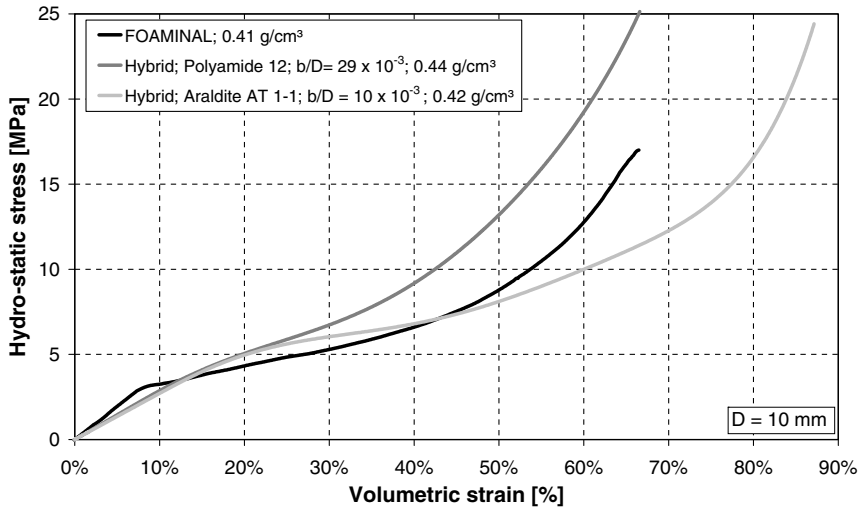

Fig. 21. Hydrostatic stress vs. volumetric strain curves of closed cell aluminum foam (FOAMINAL®) and aluminum foam-polymer hybrid samples (D = 10 mm).

parison) are subject to more pronounced strain hardening and can thus bear higher loads at elevated strain levels than brittle ones, the reason being that in the former, even at high compression, all members of the internal structure still bear load, since global deformation is based on local plastic yield rather than brittle fracture (Lehmhus and Banhart, 2003).

Comparison of conventional aluminum foams and the hybrid material revealed a difference in the stress vs. compression curves (Fig. 21). At low compression, the latter show a lower stress level than FOAMINAL®, thus matching uniaxial compression test results. Furthermore, the closed cell foam once more shows a clearly distinguishable transition from quasi-elastic to plastic deformation mode. The explanation for this effect is along the same lines as in the case of uniaxial compression. The growing difference (with increasing strain) between PA and EP bonded aluminum foam-polymer hybrid samples can partly, but not fully be explained by differences in coating thickness. The open porosity is smaller for samples having the thicker PA coating. Consequently, this open porosity reaches complete compression at lower global strain levels than is the case for samples with a thinner EP coating. The earlier densification results in the observed stress increase occurring at lower global strain values. The divergence is already visible in Fig. 20.

5. Conclusions

In the present study, mechanical strength and stiffness of APM foam under different loading conditions have been examined. The respective values fall short of conventional aluminum foams of the same matrix alloy, but only slightly in terms of

strength. Aluminum foam-polymer hybrid properties are influenced by the type of adhesive and coating thickness. Furthermore, there is the effect of (foam element) density, which is again similar to what is known from conventional aluminum foams. The influence of the foam element volume/diameter is negligible in most cases. For samples produced from larger foam elements with diameters D = 10 or 15 mm alone, random element arrangement might have been disturbed by boundary effects. Filling the comparably small sample volume (geometry: cylinder, diameter = 50 mm, height = 75 mm/50 mm) with these elements reproduced the sample geometry roughly. Therefore individual element arrangement potentially influenced mechanical properties. Further investigations with constant ratios between element and sample dimensions (e.g., 1 to 10) will provide more insight into this aspect. A noticeable effect seems possible, since deviations in element arrangement affect coordination numbers and thus contact points between a foam element and its neighbors, as well as orientation relationships.

The elemental built-up of APM foams plays a key role for mechanical performance in initial quasi-elastic deformation. Random arrays of spherical/ellipsoid aluminum foam elements are joined to each other by adhesive bonding. Approximately 40% of the hybrid volume remains as open porosity (open space between elements). The cross section of the polymer joints between foam elements is comparably small (compared to element total surface). During initial loading of the hybrid these joints are the "weakest link" in the global structure. Individual absolute joint properties (stiffness, compressive yield strength) determine global performance of the hybrid structure. Polymer coating thickness, foam element volume and density are subject to scatter. Thus properties of joints have scatter as well. With increasing load on the hybrid structure a growing number of joints transfer from quasi-elastic to plastic deformation. This effect explains the rather "soft" transition of the hybrid from quasi-elastic to plastic deformation.

In the course of compression, the difference between such localized stiffnesses/stresses and the global stiffness/stress level decreases—it disappears as soon as the initial fraction of open porosity in the sample is (predominantly) eliminated. Due to random arrangement of spheres in the hybrid material, this is typically the case at a global compressive strain level of approximately 30%. From this level onwards, the material deforms nearly identically to conventional aluminum foam.

Energy absorption levels of certain APM foams (EP bonded, $b/D = 10 \times 10^{-3}$; PA bonded, $b/D = 29 \times 10^{-3}$) reach high levels, which are competitive with conventional aluminum foams. Scatter in APM foam properties is significantly lower than in conventional aluminum foams. While it is necessary to work under a suitable safety factor in the design, the apparent advantage of conventional foams in terms of specific strength and stiffness might be lost.

References

Andrews, E., Sanders, W., Gibson, L.J., 1999. Compressive and tensile behaviour of aluminum foams. In: Mat. Sci. Eng. A270, 113–124.

Ashby, M.F., Evans, A., Fleck, N.A., Gibson, L.J., Hutchinson, J.W., Wadley, H.N.G., 2000. Metal Foams—A Design Guide. Butterworth Heinemann, ISBN 9780750672191. 2000.

Avalle, M., Diez, M., Lehmhus, D., Bosch-Rekveldt, M., Watson, J., 2004. Report on experimental results, in APROSYS Deliverable D7.1.6A, document No. AP-SP71-0027-A (2004), pp. 29–113.

Baumeister, J., 1990. German patent DE 4018360.

Degischer, H.P., Kottar, A., 1999. On the non-destructive testing of metal foams. In: Metal Foams and Porous Metal Structures. Proceedings of the international Conference Metfoam 1999. MIT-Verlag, Bremen, pp. 213–220.

Degussa, 2004. Information sheet, Vestosint Polyamid 12-Beschichtungspulver, Degussa AG, High Performance Polymers, Marl.

Gibson, L.J., Ashby, M.F., 1997. Cellular Solids—Structure and Properties, second ed. Cambridge University Press, ISBN 9780521495608. 1997.

Fleck, N.A., 1995. On the cold compaction of powders. J. Mech. Phys. Solids 43 (9), 1409–1431.

Heylinger, P.R., McMeeking, R.M., 2001. Cold plastic compaction of powders by a network model. J. Mech. Phys. Solids 49, 2031–2054.

Huschka, S., Hicken, S., Arendts, F.J., 1997. Modellierung der Spannungs-Stauchungskurven von Aluminumschaum unter Berücksichtigung der Porengrößenverteilung. In: Beiträge zum Symposium Metallschäume. MIT-Verlag, Bremen, pp. 189–197.

Issen, K.A., Casey, T.P., Dixon, D.M., Richards, M.C., Ingraham, J.P., 2005. Characterization and modeling of localized compaction in aluminum foam, In: Scripta Mat., Vol. 52, 2005, pp. 911–915.

Markaki, A.E., Clyne, T.W., 2001. The effect of cell wall microstructure on the deformation and fracture of aluminum-based foams, In: Acta Mater. Vol. 49, 2001, pp. 1677–1686.

Nusholtz, G.S., Bilkhu, S., Founas, M., Uduma, K., DeBois, P.A., 1996. Impact response of foam: the effect of the state of stress, Stapp Car Crash Conference, SAE paper 962418.

Lehmhus, D., Banhart, J., 2003. Properties of heat-treated aluminum foams. Mat. Sci. Eng. A A349, 98–110.

Peroni, L., Avalle, M., 2007. The mechanical behaviour of polyurethane foam in multiaxial loading conditions, In: Implast and Plasticity, Proceedings of the IMPLAST'07 conference, Bochum.

Rausch, G., Stöbener, K., 2006. Improving Structural Crashworthiness Using Metallic and Organic Foams, In: Porous Metals and Metal Foaming Technology, Proceedings of the International Conference "Metfoam 2005", Kyoto, Japan, The Japan Institute of Metals, Sendai, pp. 1–4.

Ruan, D., Lu, G., Wang, B., 2005. Triaxial compression of aluminum foams, In: Impact Loading of Lightweight Structures, WIT Transactions on Engineering Sciences, Vol. 49, 2005, pp. 437–449.

Simancik, F., Kovacik, J., Schörghuber, F., 1997. Porosity in complex 3D-parts prepared from aluminum foam. In: Beiträge zum Symposium Metallschäume. MIT-Verlag, Bremen, pp. 171–176.

Stöbener, K., Lehmhus, D., Zimmer, N., Baumeister, J., 2005. German patent, DE 103 28 047, 2005.

Vantico, 2001. Product data sheet„Araldite AT 1-1", publication number A405 c D, Vantico GmbH & Co KG, Wehr/Baden.